

LipDiffuser: Lip-to-Speech Generation with Conditional Diffusion Models

Danilo de Oliveira*

Julius Richter*

Tal Peer

Timo Gerkmann

Signal Processing Group
University of Hamburg

{danilo.oliveira, julius.richter, tal.peer, timo.gerkmann}@uni-hamburg.de

Abstract

We present *LipDiffuser*, a conditional diffusion model for lip-to-speech generation synthesizing natural and intelligible speech directly from silent video recordings. Our approach leverages the magnitude-preserving ablated diffusion model (MP-ADM) architecture as a denoiser model. To effectively condition the model, we incorporate visual features using magnitude-preserving feature-wise linear modulation (MP-FiLM) alongside speaker embeddings. A neural vocoder then reconstructs the speech waveform from the generated mel-spectrograms. Evaluations on *LRS3* and *TCD-TIMIT* demonstrate that *LipDiffuser* outperforms existing lip-to-speech baselines in perceptual speech quality and speaker similarity, while remaining competitive in downstream automatic speech recognition (ASR). These findings are also supported by a formal listening experiment. Extensive ablation studies and cross-dataset evaluation confirm the effectiveness and generalization capabilities of our approach.

1 Introduction

The task of conditional temporal data generation consists of creating new data sequences whose evolution over time is guided by corresponding conditioning data [1], where the generated data and conditioning information are often of different modalities. Generative models, such as conditional diffusion models [2], are particularly well suited for this task as they possess a remarkable capability to learn complex posterior distributions over possible outputs given observed conditioning data. This enables the synthesis of realistic and diverse outcomes that reflect the variability present in many real-world nonstationary data streams. Such approaches are especially relevant in multimodal applications—for example, generating synchronized video frames from an audio signal [3], or synthesizing realistic audio from corresponding visual cues [4], such as lip movements or gestural data. Additionally, these models have shown promise in medical applications, where physiological temporal signals such as electroencephalography (EEG) can be generated or imputed based on other clinical time series [5]. The main challenges in conditional temporal data generation include aligning the temporal data of different modalities and possibly different feature rates, as well as learning the intricate relationships between modalities in a robust and generalizable manner to ensure seamless integration and synchronization of the end result.

Diffusion models generate data by gradually transforming a noise sample into a sample from a given data distribution [6, 7]. This diffusion process can be formulated as a stochastic differential equation (SDE) [8], which defines the forward process describing the transition from the data distribution to a Gaussian noise distribution. While unconditional diffusion models generate a sample from the data distribution, as captured during training, conditional diffusion models add the ability to generate a sample from a conditional distribution, where the conditioning variable instructs the

*Authors contributed equally to this work.

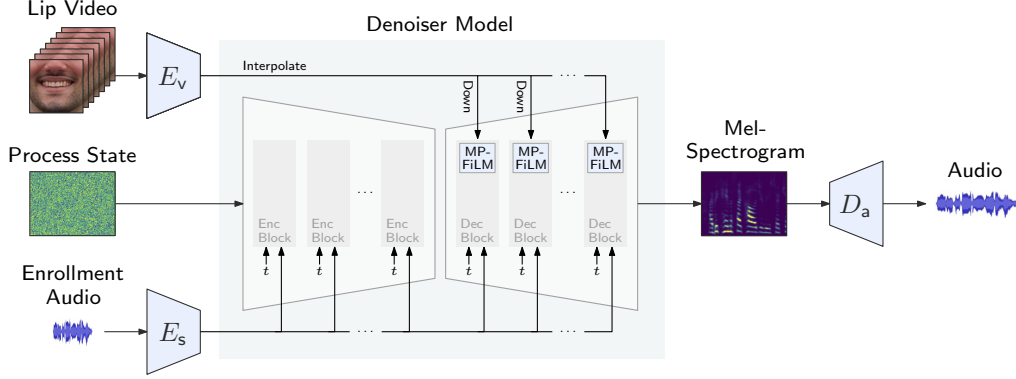


Figure 1: *LipDiffuser*: The model comprises a video encoder E_v , a speaker encoder E_s , a denoiser model, and a neural vocoder D_a . The denoiser model takes as input the process state, video features extracted by the video encoder, the current process time t , and the speaker embedding from the speaker encoder, and predicts a mel-spectrogram. The video features are interpolated to match the audio feature rate, then downsampled to the feature rate of the decoder’s target resolutions. These downsampled features are fused within the decoder blocks using magnitude-preserving feature-wise linear modulation (MP-FiLM) layers. After reverse diffusion, the neural vocoder synthesizes an audio signal from the generated mel-spectrogram. For details about the encoder and decoder blocks, see Figure 2.

model to generate a sample that matches some other information. For example, an unconditional speech model can generate audio that resembles natural speech in its acoustic properties [9], but the resulting signal typically lacks any coherent semantic content [10]. By conditioning the model on additional information, such as a text transcript, the generated speech can be guided to retain natural-sounding characteristics and accurately convey the intended meaning specified by the conditioning input [10, 11].

In this work, we develop a conditional diffusion model and apply it to the lip-to-speech task, which involves synthesizing accurate speech signals based on lip movement data captured in video. Real-world video recordings often suffer from a very low-quality audio track. This can result from a noisy recording environment, inadequate equipment, or storage media corruption. Distorted audio can be restored using speech enhancement systems, which may also harness the visual modality [12, 13], but these systems have their limits, and they tend to perform poorly in adverse noise conditions. In severe cases, the audio track may be completely unusable or even missing. In the context of human speech, visual and auditory information both play a role in the ability to understand what a person is saying [14]. However, these two modalities are not equally important; while missing visual information can lead to reduced intelligibility, the lack of audio is practically destructive to speech communication [15], except for individuals highly trained in lip reading [16].

Lip-to-speech is the process of generating a natural-sounding speech signal corresponding to a given silent video of a person speaking. Lip-to-speech systems thus restore the ability to understand human speech even in scenarios where the audio track is missing or severely distorted, including cases with negative signal-to-noise ratios (SNRs). A high-quality lip-to-speech system must ensure that the generated speech signal is intelligible, synchronized with the speaker’s lip movements, and sounds natural. Ideally, the speech signal must also match the speaker’s characteristics, including age, gender, and accent. A major challenge for lip-to-speech techniques stems from the one-to-many mapping between visemes and phonemes [17, Table 1]; different phonemes can correspond to the same sequence of lip movements, leading to ambiguity. This issue can be alleviated by including a longer temporal context in the generation process [18]. Another difficulty is alignment and synchronization of the visual cues from the lip movements with the generated audio, considering the large differences in feature rates between the visual and audio signals (e.g., 25 Hz for video compared to 48 kHz for audio).

We introduce *LipDiffuser* (Figure 1), a lip-to-speech method based on a conditional diffusion model. The proposed method comprises a video encoder, a speaker encoder, a denoiser model, and a neural vocoder. For the denoiser model, we utilize the magnitude-preserving ablated diffusion model

(MP-ADM) architecture [19], which builds upon the ablated diffusion model (ADM) architecture [20] by introducing a series of modifications that significantly enhance output quality while retaining the overall structure. During diffusion sampling, the denoiser model takes as input the current process state, video features extracted by the video encoder, the current diffusion timestep, and a speaker embedding from the speaker encoder, and predicts a mel-spectrogram. To effectively incorporate visual cues, we propose integrating video features matched via interpolation and downsampling into the denoising network’s decoder using our proposed magnitude-preserving feature-wise linear modulation (MP-FiLM) layers. After the reverse diffusion process, the neural vocoder synthesizes the final audio waveform from the generated mel-spectrogram.

We conduct our experiments on two audio-visual speech datasets: *LRS3* [21] and *TCD-TIMIT* [22]. To enable comparison with audio-visual speech enhancement methods, we create the *LRS3-CHiME3* dataset by mixing speech from *LRS3* with noise files from *CHiME3* [23] and use the *NTCD-TIMIT* benchmark [24]. Our findings suggest that lip-to-speech approaches can offer advantages over audio-visual speech enhancement, particularly when the input audio is severely degraded ($\text{SNR} < -5$ dB). Specifically, we show that our proposed *LipDiffuser* model outperforms all lip-to-speech baselines in terms of speech quality and speaker similarity, while remaining competitive in automatic speech recognition (ASR) performance and synchrony. Besides instrumental metrics, results on speech quality and speaker similarity are also supported by formal listening experiments. Furthermore, cross-dataset evaluations demonstrate the strong generalization capabilities of our method in both speech quality and speaker similarity. Finally, we conduct extensive ablation studies on data selection, input representation, and visual features to validate various design choices. Audio-visual examples, code, and pretrained checkpoints are available online.¹

2 Related work

2.1 Lip-to-speech

A range of learning-based lip-to-speech methods has been introduced in recent years. These approaches vary regarding the underlying model architectures and learning paradigms, the types of visual and additional information leveraged, and the strategies used to guide the process during training and inference.

Kim et al. [25] present *Lip2Speech*, a lip-to-speech method that includes a visual front-end, a *Conformer* model [26] for capturing temporal relationships, and a mel-spectrogram generator conditioned on speaker embeddings. They propose a multi-task learning approach that consists of: (a) a connectionist temporal classification (CTC) [27] loss between the visual representations and the text targets; (b) text prediction utilizing a pretrained ASR model; and (c) a mel-spectrogram reconstruction loss. Finally, they use the Griffin-Lim algorithm [28] to convert the mel-spectrogram into a waveform.

Choi et al. [29] propose a lip-to-speech model that employs speech representations from a self-supervised learning (SSL) model. In a multi-task learning framework, their model predicts both mel-spectrograms and speech representations derived from a pretrained SSL model. In addition, they develop a vocoder that generates the waveform with the mel-spectrogram and speech units. During training, they augment the input mel-spectrograms with blur and noise to help the vocoder learn to generate waveforms from the generated mel-spectrograms by referencing the speech units. In a follow-up work, Choi et al. [30] present *DiffV2S*, a diffusion-based lip-to-speech method based on a speaker embedding derived from the visual input. This approach addresses the challenge of inferring the speaker’s characteristics without audio.

Yemini et al. [31] introduce *LipVoicer*, a lip-to-speech method that uses a diffusion model conditioned on lip video and incorporates a classifier-guidance mechanism [20] based on text. A pretrained ASR model [32] acts as the classifier, whereas a pretrained lip-reading network [33] predicts the spoken text from the silent video, offering guidance for the score model. They train the diffusion model to generate mel-spectrograms and utilize *DiffWave* [10] as a neural vocoder to produce the raw audio.

In contrast to the above-mentioned methods, our *LipDiffuser* model achieves aligned conditioning by interpolating the video features to match the temporal resolution of the audio features within the denoiser model, and fusing them through MP-FiLM layers. In addition, we pre-enhance the audio

¹Audio-visual examples can be found on the website <https://sp-uhh.github.io/lip2speech/>

track of the “in-the-wild” audio-visual training data to increase the audio generation quality of our model, and pretrain the model with audio-only data first.

2.2 Audio-only and audio-visual speech enhancement

Speech enhancement refers to the process of improving the quality and intelligibility of a speech signal by reducing noise and reverberation [34]. Numerous computational methods have been developed for this task, most operating in the time-frequency domain using the short-time Fourier transform (STFT). Machine learning-based speech enhancement methods are commonly divided into predictive and generative learning paradigms [35], and they vary in the types of information leveraged to estimate the clean speech signal. While practical approaches often exploit multi-channel input from microphone arrays to utilize spatial information for improved performance in adverse acoustic environments [36], the present work focuses on single-channel speech enhancement, relying solely on audio captured from a single microphone.

Human perception naturally integrates auditory and visual information to enhance speech understanding, particularly in challenging listening environments [37, 38]. Neuroimaging and behavioral studies have shown that visual cues, such as a speaker’s lip movements, can significantly improve both speech intelligibility and localization [39–41]. This inherent crossmodal integration motivates the development of audio-visual speech enhancement methods, aiming to replicate these perceptual advantages in machine learning systems [12]. By leveraging both audio and visual modalities, modern systems seek to enhance speech quality and intelligibility more robustly than is possible with audio alone [13, 42, 43].

2.3 Diffusion models

Diffusion models break down data generation into more manageable denoising tasks by progressively removing noise and refining the data [6, 7]. The forward process used for training can be described by a SDE, which transforms the target distribution into a terminating Gaussian distribution, which serves as the initial distribution for sampling [8]. Reversing this process in time yields the reverse process, which is characterized by a different SDE that is numerically integrated during inference using a denoiser or score model, depending on the specifics of the sampling procedure.

The denoiser model is a neural network trained to distinguish the target data from Gaussian noise introduced during the forward process. Expressive denoiser models are often implemented using the U-Net architecture [44], augmented with self-attention layers [45]. Other approaches, such as diffusion transformers [46], exist but are outside the scope of this work. To keep network operations within an appropriate range and prevent large variations in gradient magnitudes, Karras et al. [47] proposed using time-dependent scaling of the network’s inputs and outputs, combined with a skip connection of the process state, known as preconditioning. In a subsequent study, Karras et al. [19] observed that uncontrolled changes in the magnitude and imbalances in both network activations and weights persisted throughout the training process, even when preconditioning was applied. To address this issue, they redesigned the network layers of the ADM U-Net architecture [20] to better preserve the expected magnitudes of activations, weights, and parameter updates. This adjustment led to improved performance in image generation tasks.

Conditional diffusion models extend the capabilities of standard diffusion models by incorporating additional information, such as class labels, textual descriptions, or other context, into the data generation process. This conditioning enables the model to generate data that adheres to specific requirements or mimics particular patterns, significantly enhancing its practical applicability [20]. Architecturally, conditioning is often achieved through cross-attention layers [2], or by simply concatenating or adding conditional features [13]. These approaches enable the model to focus on relevant aspects of the conditioning input throughout the denoising process.

3 Method

Figure 1 shows an overview of our model called *LipDiffuser*. The model consists of a video encoder E_v , a speaker encoder E_s , a denoiser model D_θ parameterized by θ , and a neural vocoder D_a . The denoiser model receives as inputs the process state $\mathbf{x}_t \in \mathbb{R}^{n_a}$, a speaker embedding $\mathbf{s} \in \mathbb{R}^{n_s}$ from the speaker encoder, video features $\mathbf{v} \in \mathbb{R}^{n_v}$ from the video encoder, and the process time t , and predicts the mel-spectrogram $\hat{\mathbf{x}} \in \mathbb{R}^{n_a}$.

3.1 Training objective

We use denoising score matching [48] as our training objective. For a process time t , the training objective is defined as minimizing

$$\mathcal{J}(D_\theta, t) = \mathbb{E}_{\mathbf{x}, \mathbf{n}, \mathbf{s}, \mathbf{v}} [\|D_\theta(\mathbf{x} + \mathbf{n}, \mathbf{s}, \mathbf{v}, t) - \mathbf{x}\|_2^2], \quad (1)$$

where $(\mathbf{x}, \mathbf{s}, \mathbf{v}) \sim p_{\text{data}}(\mathbf{x}, \mathbf{s}, \mathbf{v})$ is sampled from the dataset, and $\mathbf{n} \sim \mathcal{N}(\mathbf{0}, \sigma(t)\mathbf{I})$ is a random Gaussian vector with time-dependent standard deviation $\sigma(t) = t$. The overall training objective is defined as a weighted expectation of $\mathcal{J}(D_\theta, t)$ over the process time,

$$\mathcal{J}(\theta') = \mathbb{E}_t \left[\frac{\lambda(t)}{\exp u_{\tilde{\theta}}(t)} \mathcal{J}(D_\theta; t) + u_{\tilde{\theta}}(t) \right], \quad (2)$$

where $\ln(t) \sim \mathcal{N}(P_{\text{mean}}, P_{\text{std}})$ with hyperparameters P_{mean} and P_{std} , and $\lambda : \mathbb{R} \rightarrow \mathbb{R}$ is a time-dependent weight. Following uncertainty-based multi-task learning [49], the loss is further weighted by $u_{\tilde{\theta}}(t)$, a learnable linear projection of the process time parameterized by $\tilde{\theta}$, representing the uncertainty of the model. At the same time, the model is penalized for this uncertainty, encouraging $u_{\tilde{\theta}}(t)$ to be as low as possible. The full parameter set $\theta' = \{\theta, \tilde{\theta}\}$ thus includes both the denoiser model parameters and those of the learnable linear projection.

Following Karras et al. [47], we define the denoiser model D_θ as

$$D_\theta(\mathbf{x}_t, \mathbf{s}, \mathbf{v}, t) = c_{\text{skip}}(t)\mathbf{x}_t + c_{\text{out}}(t)F_\theta(c_{\text{in}}(t)\mathbf{x}_t, \mathbf{s}, \mathbf{v}, t), \quad (3)$$

where $c_{\text{skip}} : \mathbb{R} \rightarrow \mathbb{R}$ is a skip scaling controlling the skip connection of \mathbf{x}_t , $c_{\text{out}} : \mathbb{R} \rightarrow \mathbb{R}$ is an output scaling, and $c_{\text{in}} : \mathbb{R} \rightarrow \mathbb{R}$ is an input scaling. The function $F_\theta : \mathbb{R}^{n_a} \times \mathbb{R}^{n_s} \times \mathbb{R}^{n_v} \times \mathbb{R} \rightarrow \mathbb{R}^{n_a}$ is a neural network parameterized by θ .

3.2 Network architecture

We utilize the MP-ADM architecture for our neural network [19]. This architecture builds on the ADM architecture [20], introducing a series of modifications that retain the overall structure while significantly enhancing output quality. In particular, the network layers are carefully designed to preserve the expected magnitudes of activations and weight matrices during training. To condition the network on video features, we integrate feature-wise linear modulation (FiLM) [50] into the MP-ADM architecture. FiLM has been successfully applied in conditioning audio source separation [51] and speech enhancement [52] systems on language prompts, and conditioning audio on video features for audio-visual sound event recognition [53]. Here, we introduce MP-FiLM, which we motivate as follows.

Magnitude-preserving FiLM: For an input $\mathbf{x} \in \mathbb{R}^{d_x}$ and conditioning variable $\mathbf{c} \in \mathbb{R}^{d_c}$, FiLM layers are channel-wise defined as

$$\text{FiLM}(\mathbf{x}, \mathbf{c} | \theta, \phi) = \gamma_\theta(\mathbf{c}) \odot \mathbf{x} + \beta_\phi(\mathbf{c}), \quad (4)$$

where $\gamma_\theta : \mathbb{R}^{d_c} \rightarrow \mathbb{R}^{d_x}$ and $\beta_\phi : \mathbb{R}^{d_c} \rightarrow \mathbb{R}^{d_x}$ are neural networks parameterized by θ and ϕ and \odot represents the Hadamard product [50]. To ensure magnitude preservation of the addition in (4), we define MP-FiLM as

$$\text{MP-FiLM}(\mathbf{x}, \mathbf{c} | \theta, \phi) = \frac{(\mathbf{1} - \gamma_\theta(\mathbf{c})) \odot \mathbf{x} + \gamma_\theta(\mathbf{c}) \odot \beta_\phi(\mathbf{c})}{\sqrt{(\mathbf{1} - \gamma_\theta(\mathbf{c}))^2 + \gamma_\theta(\mathbf{c})^2}}. \quad (5)$$

Figure 2 shows our modified MP-ADM architecture, including MP-FiLM, which is integrated in each decoder block. Unlike the original FiLM, here the scaling and shifting of the network’s activations are conducted per frame and not globally, so that each lip movement conditions the corresponding audio frame. With that intent, video features are initially interpolated in the time dimension to match the audio frame rate. We implement β_ϕ and γ_θ with two-layered convolutional blocks, containing a convolutional layer of kernel size 5, to account for potential misalignments between audio and lip movement, followed by a pointwise convolution. The neural network γ_θ contains an additional learned gain initialized at 0, followed by a clamping operation to bound the output between 0 and 1, defining the relative contribution of the video features at each fusion stage.

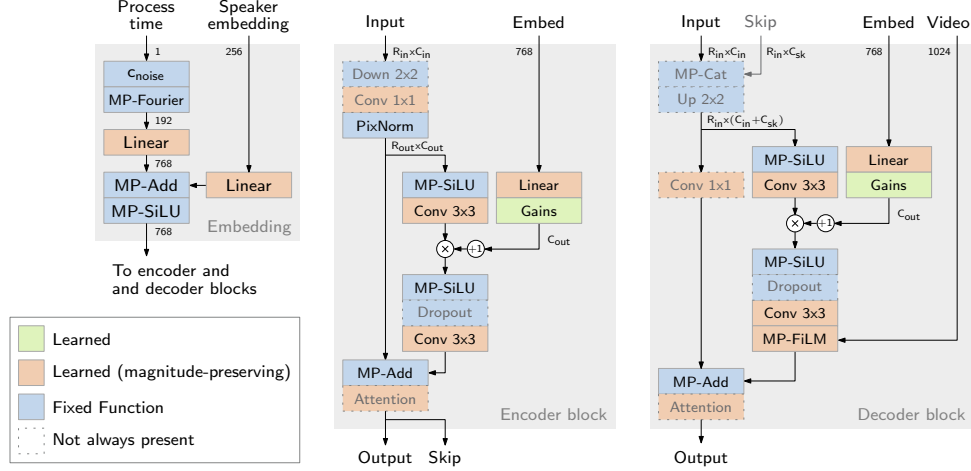


Figure 2: Modified MP-ADM network architecture with MP-FiLM layer to integrate video features.

3.3 Inference

For generating speech from video, we first extract video features $\mathbf{v} = E_v(\tilde{\mathbf{v}})$ from preprocessed video frames $\tilde{\mathbf{v}} \in \mathbb{R}^{N \times H \times W}$ using the video encoder E_v , where $\tilde{\mathbf{v}}$ is a grayscale video with N frames, height H , and width W depicting the speaker’s lip movements. We extract a speaker embedding $\mathbf{s} = E_s(\tilde{\mathbf{s}})$ using the speaker encoder E_s , where $\tilde{\mathbf{s}} \in \mathbb{R}^{n_s}$ is enrollment data of the target speaker’s voice containing n_s samples. Given the precomputed video features and the speaker embedding, we perform reverse diffusion using the trained denoiser model D_θ . We use the second-order deterministic sampler from Karras et al. [47] with $M = 32$ sampling steps to generate a mel-spectrogram $\hat{\mathbf{x}} \in \mathbb{R}^{n_a}$. Finally, we synthesize the audio signal $\tilde{\mathbf{x}} = D_a(\hat{\mathbf{x}})$ using the neural vocoder D_a , where $\tilde{\mathbf{x}} \in \mathbb{R}^{n_{\tilde{x}}}$ denotes the estimated time-domain speech signal containing $n_{\tilde{x}}$ samples.

4 Experimental setup

We train our models for 32M samples using batch size 256, reference (peak) learning rate of 0.005, with linear ramp up followed by inverse square root decay, following [19]. The optimizer is ADAM [54], with $\beta_1 = 0.9$ and $\beta_2 = 0.99$. The weighting function is $\lambda(t) = (\sigma(t)^2 + \sigma_{data}^2) / (\sigma(t) \sigma_{data})^2$, where σ_{data} is calculated on a subset of the training set. For the noise level distribution, we set $P_{mean} = -1.2$ and $P_{std} = 1.2$, following [19]. The denoiser model contains ~ 205 M parameters. Training is conducted on NVIDIA H100 graphics processing units (GPUs), typically requiring 60 GPU hours.

4.1 Data

We utilize the *LRS3* dataset [21] for training, validation, and the test. *LRS3* is an “in-the-wild” dataset comprising audio-visual recordings from TED Talks, in which the audio track often includes background noise and reverberation. Therefore, we use a pretrained generative speech enhancement model, specifically the Schrödinger bridge [55, 56], to enhance the audio tracks of the *LRS3* dataset. The preprocessing model has been trained on the *EARS-WHAM* [57] and *VB-DMD* [58] datasets, for which a checkpoint is available online.² For the method to work, we have found that an audio-only pretraining stage is required, without video conditioning features. To increase the variety and quantity of training data, we pretrain the model on the 960 hours of the *LibriSpeech* dataset [59], also preprocessed by the speech enhancement model.

We view lip-to-speech as an extreme case of audio-visual speech enhancement, where the audio is either completely absent or heavily corrupted. Consequently, we create an audio-visual speech enhancement benchmark called *LRS3-CHiME3*. This benchmark includes six subsets, each with a distinct SNR setting (5, 0, −5, −10, −15, and −20 dB). To create these subsets, we mixed clean speech from *LRS3* with noise files randomly sampled from the *CHiME3* noise database [23], adjusting

²<https://github.com/sp-uhh/sgmse>

Table 1: Results on *LRS3-CHiME3* showing mean values and standard deviation. Comparison of speech enhancement (SE) and lip-to-speech models at an SNR of -10 dB. Higher values indicate better performance except word error rate (WER). Input modalities include audio (A), video (V), enrollment audio (E), or their combinations. Enrollment audio is derived from the clean reference.

	Input	DNSMOS	NISQA	LPS	WER ↓	SpkSim	
	Clean	—	3.56 ± 0.36	4.65 ± 0.50	1.00 ± 0.00	0.09 ± 0.16	1.00 ± 0.00
	Noisy	—	2.16 ± 0.14	0.55 ± 0.27	0.11 ± 0.19	0.89 ± 0.25	0.26 ± 0.24
SE	SGMSE+	A	3.04 ± 0.35	2.73 ± 0.87	0.35 ± 0.34	0.75 ± 0.37	0.35 ± 0.23
	AV-Gen	A+V	2.90 ± 0.25	2.24 ± 0.60	0.50 ± 0.33	0.56 ± 0.37	0.36 ± 0.22
Lip-to-Speech	Lip2Speech	V+E	2.37 ± 0.13	1.42 ± 0.43	0.35 ± 0.26	0.72 ± 0.29	0.11 ± 0.11
	DiffV2S	V	3.17 ± 0.29	3.48 ± 0.52	0.45 ± 0.37	0.51 ± 0.36	0.16 ± 0.13
	IL2S	V+E	2.84 ± 0.26	2.53 ± 0.60	0.52 ± 0.27	0.59 ± 0.33	0.34 ± 0.14
	IL2S (SSL)	V+E	2.86 ± 0.28	2.62 ± 0.61	0.67 ± 0.28	0.36 ± 0.34	0.37 ± 0.14
	LipVoicer	V	3.17 ± 0.30	3.53 ± 0.64	0.57 ± 0.30	0.36 ± 0.33	0.15 ± 0.14
	LipDiffuser (ours)	V+E	3.64 ± 0.30	4.57 ± 0.52	0.64 ± 0.27	0.38 ± 0.35	0.63 ± 0.14

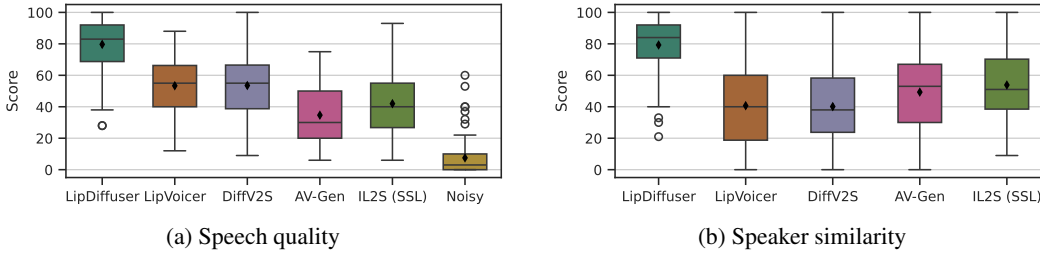


Figure 3: Results of formal listening experiments. Participants were instructed to rate the overall speech quality or speaker similarity compared to a reference on a continuous scale from 0 to 100. The boxes show the 1st and 3rd quartiles along with the median (solid line) and mean (diamond marker). The whiskers cover datapoints lying within 1.5 times the inter-quartile range from the box.

the noise levels to achieve the specified SNR for each set. For cross-dataset evaluation, we utilize all files with an SNR of -5 dB of the *NTCD-TIMIT* test set [24], which contains audio-visual recordings from the *TCD-TIMIT* dataset [22] mixed with noise from the *NOISEX-92* dataset [60] and *CHiME* challenges [23, 61].

4.2 Input representation

We use audio samples at a sampling rate of 16 kHz. We encode the waveforms into mel-spectrograms with fast Fourier transform (FFT) length of 1024, and hop length of 256 samples, thus obtaining a feature rate of 62.5 Hz. The number of mel-frequency bins per frame is $n_a = 80$. The spectrograms are scaled and shifted to be standardized to zero-mean and a variance of 0.5, based on statistics computed on the training set. The time-frequency outputs of the model are converted into a time-domain signal using the neural vocoder D_a , for which we use the *HiFi-GAN decoder* [62], pretrained at 16 kHz. Speaker embeddings are obtained via the *Wespeaker* encoder D_s [63], which encode speaker characteristics from an enrollment utterance of arbitrary length into a single feature vector of size $n_s = 256$. Video conditioning inputs are at 25 frames per second. The video frames are preprocessed to obtain the grayscale lip region-of-interest (ROI), following the pipeline in [18, 64]. The ROIs of 88×88 pixels are fed into the self-supervised model *BRAVE*n [65], which results in video features of dimension $n_v = 1024$ per video frame.

4.3 Metrics

We evaluate the proposed *LipDiffuser* method and compare it to other methods using a variety of metrics in order to capture different dimensions of performance. To evaluate speech quality, we employ two non-intrusive, deep neural network (DNN)-based speech quality assessment models, *DNSMOS* [66] and *NISQA*. Moreover, we also evaluate the speaker similarity (SpkSim), measured as the cosine similarity between speaker embeddings generated from the enrollment and synthesized

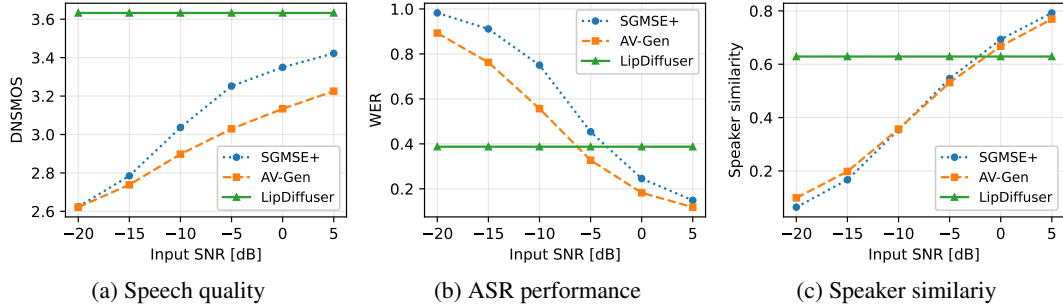


Figure 4: Performance across different dimensions—including speech quality (DNSMOS), ASR performance (WER), and speaker similarity—as a function of input SNR. Results are shown for audio-only speech enhancement (*SGMSE+*), audio-visual speech enhancement (*AV-Gen*), and lip-to-speech synthesis (*LipDiffuser*) on the *LRS3-CHiME3* dataset.

speech signals. To quantify the effect on ASR tasks, we use the QuartzNet15x5Base-En model from the *NeMo* toolkit [67] as a downstream ASR system and report the word error rate (WER). We also measure the Levenshtein phoneme similarity (LPS) using the w2v LV-60K wav2vec-based phoneme predictor [68]. In addition to instrumental metrics, we also conducted a formal listening experiment with 15 participants, using randomly selected samples from the *LRS3-CHiME3* dataset (at -10 dB SNR) and focusing on the aspects of speech quality and speaker similarity.³

4.4 Baselines

For lip-to-speech methods, we compare with *Lip2Speech* [25], *DiffV2S* [30], *IL2S* [29], and *LipVoicer* [31], all of which were trained on *LRS3*. *IL2S* comes in two configurations: the default with visual encoder trained from scratch, and a version which exploits visual features from the pretrained SSL model *AV-HuBERT* [69]. As an audio-only speech enhancement method, we utilize *SGMSE+* [70]. We retrain the model with the original hyperparameters on the *LRS3-CHiME3* dataset. As an audio-visual speech enhancement method, we employ *AV-Gen* [13]. This method integrates audio-visual features extracted from *AV-HuBERT* [69] and inputs them into *SGMSE+* [70]. We retrain the model with the original hyperparameters using the *LRS3-CHiME3* dataset.

5 Results

We begin with in-domain results using the *LRS3-CHiME3* test set comprising 1321 test files. Table 1 shows the mean performance of speech enhancement and lip-to-speech models at an SNR of -10 dB. Among the speech enhancement methods, the audio-visual *AV-Gen* model outperforms the audio-only *SGMSE+* baseline regarding WER, and LPS, highlighting the benefit of visual information. For lip-to-speech approaches, our proposed *LipDiffuser* achieves the highest speech quality scores and the strongest speaker similarity, approaching the clean reference. In terms of ASR performance, *LipDiffuser*, *LipVoicer*, and *IL2S* (SSL) achieve comparable WER and LPS, all substantially outperforming the speech enhancement methods. The results of our listening experiments, depicted in Figure 3, follow a similar trend to the instrumental metrics w.r.t. speech quality and speaker similarity, with *LipDiffuser* showing a high mean score compared to the baselines, as well as a relatively narrower score distribution for both speech quality and speaker similarity.

Figure 4 shows DNSMOS, WER, and speaker similarity for *SGMSE+*, *AV-Gen*, and *LipDiffuser* as a function of input SNR. While the performance of both speech enhancement models declines with decreasing SNR, *LipDiffuser*’s performance remains constant since it does not rely on input audio. We observe that lip-to-speech consistently outperforms speech enhancement on all metrics below certain SNR thresholds, demonstrating its superiority in severely noisy environments.

Table 2 shows performance on the *NTCD-TIMIT* test set at an SNR of -5 dB, illustrating model generalization to out-of-domain data. All models show reduced performance compared to in-domain results, with SE systems (*SGMSE+*, *AV-Gen*) offering only minor improvements over noisy audio, especially in WER and LPS. Among lip-to-speech models, *LipDiffuser* achieves the best DNSMOS,

³A detailed description of the listening experiment can be found in the supplemental material.

Table 2: Mismatched cross-dataset evaluation using the *NTCD-TIMIT* test set at an SNR of -5 dB. Values indicate the mean and standard deviation. Higher values indicate better performance for all metrics except WER. Input modalities include audio (A), video (V), enrollment audio (E), or their combinations. Enrollment audio is derived from the clean reference.

	Input	DNSMOS	NISQA	LPS	WER \downarrow	SpkSim
Clean	—	3.59 ± 0.24	3.61 ± 0.42	1.00 ± 0.00	0.14 ± 0.15	1.00 ± 0.00
Noisy	—	2.24 ± 0.17	1.02 ± 0.34	0.10 ± 0.19	0.93 ± 0.21	0.19 ± 0.22
SE	SGMSE+	2.74 ± 0.24	1.99 ± 0.41	0.11 ± 0.35	0.97 ± 0.25	0.23 ± 0.19
	AV-Gen	2.75 ± 0.25	1.98 ± 0.40	0.24 ± 0.17	0.96 ± 0.22	0.21 ± 0.18
L2S	<i>Lip2Speech</i>	2.33 ± 0.13	1.72 ± 0.41	0.31 ± 0.17	0.94 ± 0.22	-0.02 ± 0.08
	<i>LipVoicer</i>	3.41 ± 0.27	3.10 ± 0.46	0.61 ± 0.24	0.49 ± 0.35	0.07 ± 0.10
	<i>LipDiffuser</i> (ours)	3.73 ± 0.22	4.38 ± 0.46	0.52 ± 0.21	0.72 ± 0.33	0.52 ± 0.10

Table 3: Evaluation using different sources for the speaker embedding. For this analysis, a subset of the *LRS3-CHiME3* test set was used, limited to speakers with at least two utterances (the subset includes about 89% of the utterances in the complete test set).

	DNSMOS	NISQA	LPS	WER \downarrow	SpkSim
Same utterance	3.64 ± 0.30	4.58 ± 0.51	0.65 ± 0.26	0.43 ± 0.54	0.64 ± 0.14
Other utterance	3.65 ± 0.30	4.53 ± 0.56	0.64 ± 0.27	0.45 ± 0.53	0.50 ± 0.16
Enhanced utterance (-10dB)	3.50 ± 0.33	4.05 ± 0.74	0.54 ± 0.29	0.48 ± 0.36	0.29 ± 0.19
Noisy utterance (-10dB)	3.09 ± 0.38	3.27 ± 0.87	0.27 ± 0.26	0.78 ± 0.31	0.18 ± 0.18

NISQA, and speaker similarity, while *LipVoicer* provides the lowest WER and the highest LPS. Overall, *LipDiffuser* demonstrates strong robustness, maintaining high speech quality and speaker preservation even in mismatched, noisy conditions.

Table 3 investigates the effect of different enrollment utterances for speaker embedding on *LipDiffuser*’s performance. Using the very same, clean utterance as enrollment yields the best results across most metrics, including speaker similarity, intelligibility, and audio-visual synchronization. Using another clean utterance from the same speaker gives nearly identical quality but slightly reduced speaker similarity. Using either enhanced or noisy utterances for enrollment leads to noticeable drops, especially in speaker similarity and intelligibility. This highlights the benefit of clean enrollment audio for best performance, but also shows that speaker identity can still be maintained with clean utterances from other segments.

6 Limitations and social implications

LipDiffuser represents a significant advancement in lip-to-speech technology, offering promising applications such as reconstructing missing or damaged audio in crucial videos. Nevertheless, the speech it generates could potentially be used to deceive or manipulate, especially if misused by malicious actors. While our system incorporates a performant lip-reading component, it remains vulnerable to efforts aimed at producing false or misleading content. Addressing these ethical and security challenges is essential but is beyond the scope of the current work.

7 Conclusion

In this work, we proposed *LipDiffuser* a lip-to-speech diffusion model that synthesizes high-quality and intelligible speech from silent video recordings and an enrollment utterance. We proposed magnitude-preserving feature-wise linear modulation (MP-FiLM) layers for feature fusion within the magnitude-preserving ablated diffusion model (MP-ADM) network architecture. Experiments showed that below the threshold of -5 dB input SNR, *LipDiffuser* outperforms audio-visual and audio-only speech enhancement baselines. We conducted extensive experiments and ablations, with same- and cross-dataset evaluations. *LipDiffuser* consistently outperforms lip-to-speech baselines in audio quality and speaker similarity, with some robustness w.r.t different enrollment utterance scenarios. *LipDiffuser* demonstrates the capabilities of conditional diffusion models for generating high-quality speech in the lip-to-speech task.

References

- [1] Yiyuan Yang, Ming Jin, Haomin Wen, Chaoli Zhang, Yuxuan Liang, Lintao Ma, Yi Wang, Chenghao Liu, Bin Yang, Zenglin Xu, et al. A survey on diffusion models for time series and spatio-temporal data. *arXiv preprint arXiv:2404.18886*, 2024.
- [2] Robin Rombach, Andreas Blattmann, Dominik Lorenz, Patrick Esser, and Björn Ommer. High-resolution image synthesis with latent diffusion models. In *IEEE/CVF Conf. on Computer Vision and Pattern Recognition (CVPR)*, pages 10684–10695, 2022.
- [3] Wenxuan Zhang, Xiaodong Cun, Xuan Wang, Yong Zhang, Xi Shen, Yu Guo, Ying Shan, and Fei Wang. SadTalker: Learning realistic 3D motion coefficients for stylized audio-driven single image talking face animation. In *IEEE/CVF Conf. on Computer Vision and Pattern Recognition (CVPR)*, pages 8652–8661, 2023.
- [4] Ilpo Virtola, Vladimir Iashin, and Esa Rahtu. Temporally aligned audio for video with autoregression. In *IEEE Int. Conf. on Acoustics, Speech and Signal Process. (ICASSP)*, pages 1–5. IEEE, 2025.
- [5] Szabolcs Torma and Luca Szegletes. Generative modeling and augmentation of EEG signals using improved diffusion probabilistic models. *Journal of Neural Engineering*, 22(1):016001, 2025.
- [6] Jascha Sohl-Dickstein, Eric Weiss, Niru Maheswaranathan, and Surya Ganguli. Deep unsupervised learning using nonequilibrium thermodynamics. *Int. Conf. on Machine Learning (ICML)*, pages 2256–2265, 2015.
- [7] Jonathan Ho, Ajay Jain, and Pieter Abbeel. Denoising diffusion probabilistic models. *Advances in Neural Inf. Proc. Systems (NeurIPS)*, 33:6840–6851, 2020.
- [8] Yang Song, Jascha Sohl-Dickstein, Diederik P Kingma, Abhishek Kumar, Stefano Ermon, and Ben Poole. Score-based generative modeling through stochastic differential equations. *Int. Conf. on Learning Representations (ICLR)*, 2021.
- [9] Danilo de Oliveira, Julius Richter, Jean-Marie Lemerrier, Simon Welker, and Timo Gerkmann. Non-intrusive speech quality assessment with diffusion models trained on clean speech. *arXiv preprint arXiv:2410.17834*, 2024.
- [10] Zhifeng Kong, Wei Ping, Jiaji Huang, Kexin Zhao, and Bryan Catanzaro. DiffWave: A versatile diffusion model for audio synthesis. In *Int. Conf. on Learning Representations (ICLR)*, 2021.
- [11] Nanxin Chen, Yu Zhang, Heiga Zen, Ron J Weiss, Mohammad Norouzi, and William Chan. WaveGrad: Estimating gradients for waveform generation. In *Int. Conf. on Learning Representations (ICLR)*, 2021.
- [12] Laurent Girin, Gang Feng, and Jean-Luc Schwartz. Noisy speech enhancement with filters estimated from the speaker’s lips. In *European Conference on Speech Communication and Technology*, 1995.
- [13] Julius Richter, Simone Frintrop, and Timo Gerkmann. Audio-visual speech enhancement with score-based generative models. In *ITG Conference on Speech Communication*, pages 275–279, 2023. doi: 10.30420/456164054.
- [14] Harry McGurk and John MacDonald. Hearing lips and seeing voices. *Nature*, 264(5588):746–748, 1976.
- [15] Barbara Dodd. The role of vision in the perception of speech. *Perception*, 6(1):31–40, 1977.
- [16] Barbara Ed Dodd and Ruth Ed Campbell. *Hearing by eye: The psychology of lip-reading*. Lawrence Erlbaum Associates, Inc, 1987.
- [17] Julius Richter, Jeanine Liebold, and Timo Gerkamnn. Continuous phoneme recognition based on audio-visual modality fusion. In *International Joint Conference on Neural Networks*, pages 1–8. IEEE, 2022.
- [18] Brais Martinez, Pingchuan Ma, Stavros Petridis, and Maja Pantic. Lipreading using temporal convolutional networks. In *IEEE Int. Conf. on Acoustics, Speech and Signal Process. (ICASSP)*, pages 6319–6323. IEEE, 2020.
- [19] Tero Karras, Miika Aittala, Jaakko Lehtinen, Janne Hellsten, Timo Aila, and Samuli Laine. Analyzing and improving the training dynamics of diffusion models. In *IEEE/CVF Conf. on Computer Vision and Pattern Recognition (CVPR)*, pages 24174–24184, 2024.
- [20] Prafulla Dhariwal and Alexander Nichol. Diffusion models beat GANs on image synthesis. *Advances in Neural Inf. Proc. Systems (NeurIPS)*, 34:8780–8794, 2021.

- [21] Triantafyllos Afouras, Joon Son Chung, and Andrew Zisserman. LRS3-TED: A large-scale dataset for visual speech recognition. *arXiv preprint arXiv:1809.00496*, 2018.
- [22] Naomi Harte and Eoin Gillen. TCD-TIMIT: An audio-visual corpus of continuous speech. *IEEE Transactions on Multimedia*, 17(5):603–615, 2015.
- [23] Jon Barker, Ricard Marxer, Emmanuel Vincent, and Shinji Watanabe. The third ‘CHiME’ speech separation and recognition challenge: Dataset, task and baselines. *IEEE Workshop on Automatic Speech Recognition and Understanding (ASRU)*, pages 504–511, 2015.
- [24] Ahmed Hussen Abdelaziz et al. NTCD-TIMIT: A new database and baseline for noise-robust audio-visual speech recognition. In *ISCA Interspeech*, pages 3752–3756, 2017.
- [25] Minsu Kim, Joanna Hong, and Yong Man Ro. Lip-to-speech synthesis in the wild with multi-task learning. In *IEEE Int. Conf. on Acoustics, Speech and Signal Process. (ICASSP)*, pages 1–5, 2023.
- [26] Anmol Gulati, James Qin, Chung-Cheng Chiu, Niki Parmar, Yu Zhang, Jiahui Yu, Wei Han, Shibo Wang, Zhengdong Zhang, Yonghui Wu, et al. Conformer: Convolution-augmented transformer for speech recognition. In *ISCA Interspeech*, pages 5036–5040, 2020.
- [27] Alex Graves, Santiago Fernández, Faustino Gomez, and Jürgen Schmidhuber. Connectionist temporal classification: Labelling unsegmented sequence data with recurrent neural networks. In *Int. Conf. on Machine Learning (ICML)*, pages 369–376, 2006.
- [28] Daniel Griffin and Jae Lim. Signal estimation from modified short-time fourier transform. *IEEE Trans. on Audio, Speech, and Lang. Process. (TASLP)*, 32(2):236–243, 1984.
- [29] Jeongsoo Choi, Minsu Kim, and Yong Man Ro. Intelligible lip-to-speech synthesis with speech units. In *ISCA Interspeech*, pages 4349–4353, 2023.
- [30] Jeongsoo Choi, Joanna Hong, and Yong Man Ro. Diffv2s: Diffusion-based video-to-speech synthesis with vision-guided speaker embedding. In *IEEE/CVF Int. Conf. on Computer Vision (ICCV)*, pages 7812–7821, 2023.
- [31] Yochai Yemini, Aviv Shamsian, Lior Bracha, Sharon Gannot, and Ethan Fetaya. LipVoicer: Generating speech from silent videos guided by lip reading. In *Int. Conf. on Learning Representations (ICLR)*, 2024.
- [32] Maxime Burchi and Radu Timofte. Audio-visual efficient conformer for robust speech recognition. In *IEEE/CVF Winter Conference on Applications of Computer Vision*, pages 2258–2267, 2023.
- [33] Pingchuan Ma, Alexandros Haliassos, Adriana Fernandez-Lopez, Honglie Chen, Stavros Petridis, and Maja Pantic. Auto-AVSR: Audio-visual speech recognition with automatic labels. In *IEEE Int. Conf. on Acoustics, Speech and Signal Process. (ICASSP)*, pages 1–5. IEEE, 2023.
- [34] Emmanuel Vincent, Tuomas Virtanen, and Sharon Gannot. *Audio source separation and speech enhancement*. John Wiley & Sons, 2018.
- [35] Jean-Marie Lemerrier, Julius Richter, Simon Welker, Eloi Moliner, Vesa Välimäki, and Timo Gerkmann. Diffusion models for audio restoration: A review. *IEEE Signal Processing Magazine*, 41(6):72–84, 2025.
- [36] Kristina Tesch and Timo Gerkmann. Insights into deep non-linear filters for improved multi-channel speech enhancement. *IEEE Trans. on Audio, Speech, and Lang. Process. (TASLP)*, 31:563–575, 2022.
- [37] BE Stein. *The Merging of the Senses*. MIT Press, 1993.
- [38] Ladan Shams and Aaron R Seitz. Benefits of multisensory learning. *Trends in cognitive sciences*, 12(11): 411–417, 2008.
- [39] Gemma A Calvert, Edward T Bullmore, Michael J Brammer, Ruth Campbell, Steven CR Williams, Philip K McGuire, Peter WR Woodruff, Susan D Iversen, and Anthony S David. Activation of auditory cortex during silent lipreading. *Science*, 276(5312):593–596, 1997.
- [40] William H Sumby and Irwin Pollack. Visual contribution to speech intelligibility in noise. *The journal of the acoustical society of america*, 26(2):212–215, 1954.
- [41] John J McDonald, Wolfgang A Teder-SaĖlejaĖrvi, and Steven A Hillyard. Involuntary orienting to sound improves visual perception. *Nature*, 407(6806):906–908, 2000.

- [42] Ariel Ephrat, Inbar Mosseri, Oran Lang, Tali Dekel, Kevin Wilson, Avinatan Hassidim, William T Freeman, and Michael Rubinstein. Looking to listen at the cocktail party: a speaker-independent audio-visual model for speech separation. *ACM Transactions on Graphics (TOG)*, 37(4):1–11, 2018.
- [43] Triantafyllos Afouras, Joon Son Chung, and Andrew Zisserman. The conversation: Deep audio-visual speech enhancement. *ISCA Interspeech*, pages 3244–3248, 2018.
- [44] Olaf Ronneberger, Philipp Fischer, and Thomas Brox. U-Net: Convolutional networks for biomedical image segmentation. In *Medical image computing and computer-assisted intervention*, pages 234–241. Springer, 2015.
- [45] Ashish Vaswani, Noam Shazeer, Niki Parmar, Jakob Uszkoreit, Llion Jones, Aidan N Gomez, Łukasz Kaiser, and Illia Polosukhin. Attention is all you need. *Advances in Neural Inf. Proc. Systems (NeurIPS)*, 30, 2017.
- [46] William Peebles and Saining Xie. Scalable diffusion models with transformers. In *IEEE/CVF Int. Conf. on Computer Vision (ICCV)*, pages 4195–4205, 2023.
- [47] Tero Karras, Miika Aittala, Timo Aila, and Samuli Laine. Elucidating the design space of diffusion-based generative models. *Advances in Neural Inf. Proc. Systems (NeurIPS)*, 35:26565–26577, 2022.
- [48] Pascal Vincent. A connection between score matching and denoising autoencoders. *Neural computation*, 23(7):1661–1674, 2011.
- [49] Alex Kendall, Yarin Gal, and Roberto Cipolla. Multi-task learning using uncertainty to weigh losses for scene geometry and semantics. In *IEEE/CVF Conf. on Computer Vision and Pattern Recognition (CVPR)*, pages 7482–7491, 2018.
- [50] Ethan Perez, Florian Strub, Harm de Vries, Vincent Dumoulin, and Aaron Courville. FiLM: Visual reasoning with a general conditioning layer. *Proceedings of the AAAI Conference on Artificial Intelligence*, 32(1), Apr. 2018. doi: 10.1609/aaai.v32i1.11671.
- [51] Xubo Liu, Haohe Liu, Qiuqiang Kong, Xinhao Mei, Jinzheng Zhao, Qiushi Huang, Mark D. Plumbley, and Wenwu Wang. Separate what you describe: Language-queried audio source separation. In *ISCA Interspeech*, pages 1801–1805, 2022. doi: 10.21437/Interspeech.2022-10894.
- [52] Danilo de Oliveira, Eric Grinstein, Patrick A. Naylor, and Timo Gerkmann. Laser: Language-queried speech enhancer. In *Int. Workshop on Acoustic Signal Enhancement (IWAENC)*, pages 90–94, 2024. doi: 10.1109/IWAENC61483.2024.10694503.
- [53] Mathilde Brousmiche, Jean Rouat, and Stéphane Dupont. Multimodal attentive fusion network for audio-visual event recognition. *Information Fusion*, 85:52–59, 2022. ISSN 1566-2535. doi: <https://doi.org/10.1016/j.inffus.2022.03.001>.
- [54] Diederik P. Kingma and Jimmy Ba. Adam: A method for stochastic optimization. In *Int. Conf. on Learning Representations (ICLR)*, 2015.
- [55] Ante Jukić, Roman Korostik, Jagadeesh Balam, and Boris Ginsburg. Schrödinger bridge for generative speech enhancement. In *ISCA Interspeech*, pages 1175–1179, 2024. doi: 10.21437/Interspeech.2024-579.
- [56] Julius Richter, Danilo de Oliveira, and Timo Gerkmann. Investigating training objectives for generative speech enhancement. *IEEE Int. Conf. on Acoustics, Speech and Signal Process. (ICASSP)*, 2025.
- [57] Julius Richter, Yi-Chiao Wu, Steven Krenn, Simon Welker, Bunlong Lay, Shinjii Watanabe, Alexander Richard, and Timo Gerkmann. EARS: An anechoic fullband speech dataset benchmarked for speech enhancement and dereverberation. In *ISCA Interspeech*, pages 4873–4877, 2024.
- [58] Cassia Valentini-Botinhao, Xin Wang, Shinji Takaki, and Junichi Yamagishi. Investigating RNN-based speech enhancement methods for noise-robust text-to-speech. *ISCA Speech Synthesis Workshop*, pages 146–152, 2016.
- [59] Vassil Panayotov, Guoguo Chen, Daniel Povey, and Sanjeev Khudanpur. Librispeech: An asr corpus based on public domain audio books. In *IEEE Int. Conf. on Acoustics, Speech and Signal Process. (ICASSP)*, pages 5206–5210, 2015. doi: 10.1109/ICASSP.2015.7178964.
- [60] Andrew Varga and Herman JM Steeneken. Assessment for automatic speech recognition: Ii. noisex-92: A database and an experiment to study the effect of additive noise on speech recognition systems. *Speech communication*, 12(3):247–251, 1993.

- [61] Emmanuel Vincent, Jon Barker, Shinji Watanabe, Jonathan Le Roux, Francesco Nesta, and Marco Matasoni. The second ‘chime’ speech separation and recognition challenge: Datasets, tasks and baselines. In *IEEE Int. Conf. on Acoustics, Speech and Signal Process. (ICASSP)*, pages 126–130, 2013.
- [62] Jungil Kong, Jaehyeon Kim, and Jaekyoung Bae. Hifi-gan: Generative adversarial networks for efficient and high fidelity speech synthesis. In H. Larochelle, M. Ranzato, R. Hadsell, M.F. Balcan, and H. Lin, editors, *Advances in Neural Inf. Proc. Systems (NeurIPS)*, volume 33, pages 17022–17033. Curran Associates, Inc., 2020.
- [63] Hongji Wang, Chengdong Liang, Shuai Wang, Zhengyang Chen, Binbin Zhang, Xu Xiang, Yanlei Deng, and Yanmin Qian. Wespeaker: A research and production oriented speaker embedding learning toolkit. In *IEEE Int. Conf. on Acoustics, Speech and Signal Process. (ICASSP)*, pages 1–5. IEEE, 2023.
- [64] Pingchuan Ma, Stavros Petridis, and Maja Pantic. End-to-end audio-visual speech recognition with conformers. In *IEEE Int. Conf. on Acoustics, Speech and Signal Process. (ICASSP)*, pages 7613–7617. IEEE, 2021.
- [65] Alexandros Haliassos, Andreas Zinonos, Rodrigo Mira, Stavros Petridis, and Maja Pantic. Braven: Improving self-supervised pre-training for visual and auditory speech recognition. In *IEEE Int. Conf. on Acoustics, Speech and Signal Process. (ICASSP)*, pages 11431–11435, 2024. doi: 10.1109/ICASSP48485.2024.10448473.
- [66] Chandan KA Reddy, Vishak Gopal, and Ross Cutler. DNSMOS: A non-intrusive perceptual objective speech quality metric to evaluate noise suppressors. In *IEEE Int. Conf. on Acoustics, Speech and Signal Process. (ICASSP)*, pages 6493–6497, 2021.
- [67] Oleksii Kuchaiev, Jason Li, Huyen Nguyen, Oleksii Hrinchuk, Ryan Leary, Boris Ginsburg, Samuel Kriman, Stanislav Beliaev, Vitaly Lavrukhin, Jack Cook, et al. NeMo: a toolkit for building AI applications using neural modules. *arXiv preprint arXiv:1909.09577*, 2019.
- [68] Jan Pirklbauer, Marvin Sach, Kristoff Fluyt, Wouter Tirry, Wafaa Wardah, Sebastian Moeller, and Tim Fingscheidt. Evaluation metrics for generative speech enhancement methods: Issues and perspectives. In *ITG Conference on Speech Communication*, pages 265–269. VDE, 2023.
- [69] Bowen Shi, Wei-Ning Hsu, Kushal Lakhotia, and Abdelrahman Mohamed. Learning audio-visual speech representation by masked multimodal cluster prediction. In *Int. Conf. on Learning Representations (ICLR)*, 2022.
- [70] Julius Richter, Simon Welker, Jean-Marie Lemerrier, Bunlong Lay, and Timo Gerkmann. Speech enhancement and dereverberation with diffusion-based generative models. *IEEE Trans. on Audio, Speech, and Lang. Process. (TASLP)*, 31:2351–2364, 2023. doi: 10.1109/TASLP.2023.3285241.
- [71] Joon Son Chung and Andrew Zisserman. Out of time: automated lip sync in the wild. In *Asian Conference on Computer Vision Workshops*, pages 251–263. Springer, 2017.
- [72] KR Prajwal, Rudrabha Mukhopadhyay, Vinay P Namboodiri, and CV Jawahar. A lip sync expert is all you need for speech to lip generation in the wild. In *Proceedings of the 28th ACM international conference on multimedia*, pages 484–492, 2020.
- [73] Rithesh Kumar, Prem Seetharaman, Alejandro Luebs, Ishaan Kumar, and Kundan Kumar. High-fidelity audio compression with improved rvqgan. In *Advances in Neural Inf. Proc. Systems (NeurIPS)*. Curran Associates Inc., 2023.
- [74] Alexandros Haliassos, Rodrigo Mira, Honglie Chen, Zoe Landgraf, Stavros Petridis, and Maja Pantic. Unified speech recognition: A single model for auditory, visual and audiovisual inputs. 2024.
- [75] Julius Richter, Danilo de Oliveira, and Timo Gerkmann. Normalize everything: A preconditioned magnitude-preserving architecture for diffusion-based speech enhancement. *arXiv preprint arXiv:2505.05216*, 2025.

A Synchronicity

To quantitatively evaluate the temporal alignment between the generated speech and the corresponding lip movements, we employ automatic lip-sync metrics derived from *SyncNet* [71]. *SyncNet* is a widely adopted DNN designed to embed both visual and auditory speech representations in a shared space, enabling the assessment of how well the movements of the mouth in video correspond to the accompanying audio.

Specifically, we utilize two established metrics, both calculated using a pre-trained, publicly available *SyncNet* model. Lip sync error distance (LSE-D) calculates the mean distance between feature embeddings of the video frames (focused on the mouth region) and their paired audio segment [72]. A lower LSE-D value indicates a closer match and thus more accurate synchronization between the predicted speech and the visible articulatory movements. Lip sync error confidence (LSE-C) reflects the average confidence with which *SyncNet* can associate each video-audio pair as being in sync [72]. Higher confidence scores indicate better temporal alignment between the mouth movements and the generated speech signal, whereas lower values suggest potential misalignment or asynchronous output.

These metrics offer a targeted evaluation of audio-visual synchronization, overcoming the limitations of traditional image quality measures (such as SSIM or PSNR) and even lip landmark-based approaches, which may not always reliably capture subtle misalignments between speech and lip motion in synthetic or unconstrained videos. However, it is important to note that LSE-D and LSE-C are not without limitations. *SyncNet* was introduced nearly a decade ago and does not reflect the most recent advances in audio-visual correspondence or large-scale self-supervised learning. Consequently, while LSE-D and LSE-C are widely used and still provide valuable insights, their reliability and sensitivity may be limited on highly diverse data.

We report synchronicity results in Table 4 for both the *LRS3-CHiME3* (matched) and *NTCD-TIMIT* (mismatched) test sets. Across all methods and conditions, lip-to-speech models generally achieve higher LSE-C and lower LSE-D values than speech enhancement models, suggesting improved audio-visual alignment according to the *SyncNet*-based metrics. Our proposed model, *LipDiffuser*, performs comparably to other lip-to-speech baselines. Particularly on the mismatched *NTCD-TIMIT* dataset, *LipDiffuser* shows competitive LSE-D and LSE-C scores. Notably, although small differences between the top-performing approaches (e.g., *IL2S*, *DiffV2S*, and *LipDiffuser*) exist, through subjective evaluation, we found these methods to be qualitatively indistinguishable in terms of perceptual synchronization, and we did not observe meaningful discrepancies in audio-visual alignment. The numerical differences likely stem from specific inductive biases of the DNNs underpinning the *SyncNet* metric, rather than corresponding to genuine perceptual differences. This underscores the limitation of current automated lip-sync evaluation methods and highlights the ongoing need for metrics that correspond more closely to human perception.

Table 4: Results on *LRS3-CHiME3* (matched) and *NTCD-TIMIT* (mismatched) showing mean values. Comparison of speech enhancement (SE) and lip-to-speech models at an SNR of -10 dB for *LRS3-CHiME* and -5 dB for *NTCD-TIMIT*. For LSE-C, higher values indicate better performance, while for LSE-D lower is better. Input modalities include audio (A), video (V), enrollment audio (E), or their combinations. Enrollment audio is derived from the clean reference.

		LRS3-CHiME3		NTCD-TIMIT		
		Input	LSE-C	LSE-D ↓	LSE-C	LSE-D ↓
Clean		-	7.49 ± 1.60	7.10 ± 0.96	2.62 ± 1.62	9.01 ± 1.67
Noisy		-	2.03 ± 1.57	11.15 ± 1.53	0.87 ± 0.51	8.11 ± 1.45
SE	<i>SGMSE+</i>	A	4.79 ± 2.01	9.40 ± 1.63	1.16 ± 0.73	9.81 ± 1.48
	<i>AV-Gen</i>	A+V	6.40 ± 1.66	7.76 ± 1.06	1.72 ± 1.05	8.46 ± 1.41
Lip-to-Speech	<i>Lip2Speech</i>	V+E	4.29 ± 2.43	9.04 ± 1.44	2.44 ± 1.25	8.14 ± 1.20
	<i>DiffV2S</i>	V	7.28 ± 1.68	7.27 ± 1.02	-	-
	<i>IL2S</i>	V+E	8.08 ± 1.63	6.51 ± 0.90	-	-
	<i>IL2S</i> (SSL)	V+E	8.03 ± 1.61	6.54 ± 0.90	-	-
	<i>LipVoicer</i>	V	6.40 ± 1.86	8.12 ± 1.22	2.00 ± 1.26	10.67 ± 1.40
	<i>LipDiffuser</i> (ours)	V+E	6.84 ± 1.60	7.78 ± 0.93	2.29 ± 1.34	9.77 ± 1.37

B Audio-only generation

We perform a comparison of different audio feature representations for the diffusion model. We compare the mel-spectrogram features with a *HiFi-GAN* decoder [62], which is the representation employed in *LipDiffuser*, complex spectrograms denoted here as STFT features, and descript audio codec (DAC) latent features [73]. All encoder/decoder pairs we compared operate at a sampling rate of 16 kHz

The parametrization of the STFT encoder/decoder pair follows that of Richter et al. [70], with a window length of 510 samples, hop length of 128 samples, and an amplitude transformation $\tilde{c} = \beta|c|^\alpha e^{i\angle c}$, where $\beta = 0.5$ and $\alpha = 0.15$.

The DAC encoder has a hop length of 320 samples, and we use its projected latents, which are feature vectors of size 96. Table 5 shows the result using DNSMOS, NISQA, and SpkSim. Overall, the mel-spectrogram features achieve a good balance between interpretability, compactness, and output quality, obtaining the best performance across all metrics.

Table 5: Input feature comparison for audio-only speech generation on the LRS3-CHiME3 test set.

	DNSMOS	NISQA	SpkSim
Mel	3.59 ± 0.32	4.44 ± 0.48	0.53 ± 0.16
STFT	3.41 ± 0.29	3.84 ± 0.76	0.41 ± 0.14
DAC	3.07 ± 0.33	2.81 ± 0.90	0.30 ± 0.18

C Architectural search

Table 6 reports the effects of various design choices on *LipDiffuser*’s performance. Training on the original *LRS3* audio data instead of pre-enhancing the data causes a clear drop in all metrics, including speech quality, ASR performance, and speaker similarity.

Using mel-spectrograms as input representation consistently outperforms other representations, such as complex-valued spectrograms using the STFT or the DAC audio codec [73], across all metrics

Pretraining on *LRS3* instead of *LibriSpeech*, or adding FiLM layers to the encoder, yields minimal impact, indicating some flexibility in these components.

Using a checkpoint from *BRAVE*n that is finetuned on visual speech recognition (VSR) as the video encoder yields similar results, but slightly reduces the WER. Replacing the *BRAVE*n video encoder [65] with the *USR* encoder [74] yields similar quality and speaker similarity scores, but results in higher WER and lower LPS. Similar behavior can be observed using AV-HuBERT [69] as a video encoder. These effects may result from fine-tuning on VSR, variations in feature fusion methods, and the use of different self-supervised learning techniques.

Table 6: Design choice ablations on the LRS3-CHiME3 test set.

	DNSMOS	NISQA	LPS	WER ↓	SpkSim
<i>LipDiffuser</i> (Mel, BRAVE _n)	3.64 ± 0.30	4.57 ± 0.52	0.64 ± 0.27	0.38 ± 0.35	0.63 ± 0.14
– pre-enhanced training data	3.24 ± 0.25	2.98 ± 0.47	0.34 ± 0.29	0.60 ± 0.33	0.32 ± 0.14
+ LRS3 pretraining (– LibriSpeech)	3.63 ± 0.30	4.54 ± 0.54	0.63 ± 0.27	0.38 ± 0.35	0.63 ± 0.14
+ FiLM also in encoder	3.64 ± 0.30	4.57 ± 0.54	0.64 ± 0.27	0.38 ± 0.35	0.64 ± 0.14
+ STFT (– Mel)	3.37 ± 0.33	4.29 ± 0.72	0.55 ± 0.30	0.48 ± 0.37	0.51 ± 0.15
+ DAC (– Mel)	3.22 ± 0.27	2.96 ± 0.91	0.59 ± 0.30	0.42 ± 0.35	0.46 ± 0.15
+ BRAVE _n finetuned	3.63 ± 0.31	4.57 ± 0.51	0.62 ± 0.27	0.42 ± 0.35	0.63 ± 0.14
+ AV-HuBERT finetuned (– BRAVE _n)	3.66 ± 0.29	4.56 ± 0.53	0.50 ± 0.26	0.61 ± 0.34	0.62 ± 0.14
+ USR finetuned (– BRAVE _n)	3.66 ± 0.29	4.58 ± 0.52	0.43 ± 0.25	0.71 ± 0.33	0.61 ± 0.14

D Exponential moving average (EMA)

Exponential moving average (EMA) is frequently employed during the training of diffusion models to produce a smoothed estimate of the model parameters, denoted as $\hat{\theta}$. This approach, motivated by findings in stochastic optimization [54], involves maintaining an exponentially weighted average of recent parameter values to reduce the noise inherent in stochastic approximation and often leads to improved generalization compared to using only the final iterate. During each iteration n , this average is updated via the recurrence

$$\hat{\theta}_{\beta}^{(n)} = \beta \hat{\theta}_{\beta}^{(n-1)} + (1 - \beta) \theta^{(n)}, \quad (6)$$

where β (typically a value close to 1) controls the degree of exponential smoothing, gradually reducing the influence of distant past parameters.

Instead of a fixed exponential decay rate, Karras et al. [19] modified the traditional EMA by leveraging decay rates derived from power-law functions. In the power function EMA, the decay coefficient β_{γ} becomes dependent on the training iteration n , resulting in the update rule

$$\hat{\theta}_{\gamma}^{(n)} = \beta_{\gamma}^{(n)} \hat{\theta}_{\gamma}^{(n-1)} + (1 - \beta_{\gamma}^{(n)}) \theta^{(n)}, \quad \text{where} \quad \beta_{\gamma}^{(n)} = (1 - 1/n)^{\gamma+1}, \quad (7)$$

with parameter γ adjusting the sharpness and range of the averaging effect. Unlike the standard EMA in Equation (6), the power-law EMA in Equation (7) discards the random initialization $\theta^{(0)}$ altogether, attributing it no weight at the start of training. While γ offers precise mathematical control over the profile, its direct impact is not always intuitive. To facilitate interpretation, the authors describe the averaging profile using the relative standard deviation σ_{rel} , which expresses the effective width of the profile relative to the entire training trajectory. This quantity is also referred to as the EMA length. For instance, an EMA length covering 10% of the training steps corresponds to $\sigma_{\text{rel}} = 0.10$ (which translates to $\gamma \approx 6.94$).

Karras et al. [19] propose a post-training approximation technique to further explore the influence of different EMA profiles on model performance. This approach enables flexible, fine-grained adjustments of the EMA window after training has concluded. Specifically, two sets of model snapshots $\hat{\theta}_{\gamma_1}$ and $\hat{\theta}_{\gamma_2}$, computed with $\gamma_1 = 16.97$ ($\sigma_{\text{rel}} = 0.05$) and $\gamma_2 = 6.94$ ($\sigma_{\text{rel}} = 0.10$), are periodically saved during training. Afterward, parameter vectors corresponding to arbitrary EMA profiles can be estimated by constructing an optimal linear combination of the stored snapshots via least squares, aligning as closely as possible to a desired weighting scheme.

In this paper, except where explicitly indicated otherwise, we employ the directly saved snapshot with EMA length of 0.10. Nevertheless, motivated by Richter et al. [75], we analyze speech metrics on different reconstructed EMA profiles. With the *post-hoc* EMA reconstruction technique introduced by Karras et al. [19], Figure 5 shows five selected metrics as a function of the EMA length. We can notice a trend of increasing performance with increasingly longer EMA lengths, except for NISQA, which starts decreasing after 0.03. Nevertheless, the changes in absolute scale are minor, especially for changes in EMAs longer than 0.10.

E Magnitude-preserving feature-wise linear modulation (MP-FiLM)

Karras et al. [19, Appendix B.7] derives a magnitude-preserving formulation for the weighted sum of two standardized random vectors. In our case, it would be $\mathbf{x}_{\text{cond}} = w_x \mathbf{x} + w_{\beta} \beta_{\phi}(\mathbf{c})$. Assuming that the elements within each vector have equal expected magnitude and that \mathbf{x} and $\beta_{\phi}(\mathbf{c})$ are uncorrelated,

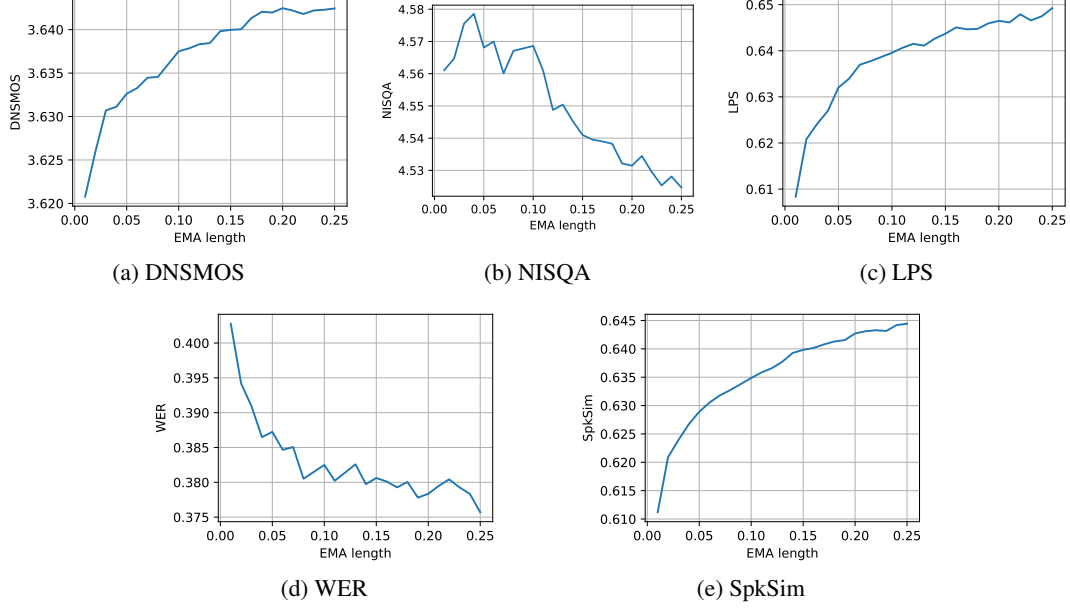


Figure 5: Selected evaluation metrics plotted as a function of EMA length. Most metrics exhibit improved performance with increasing EMA length, though NISQA peaks around an EMA length of 0.03 before declining. Overall, changes remain minor in absolute terms, particularly for EMA lengths greater than 0.10.

we have

$$\mathcal{M}[\mathbf{x}_{\text{cond}}]^2 = \frac{1}{N_c} \sum_{i=1}^{N_c} \mathbb{E}[(w_x x_i + w_\beta \beta_\phi(c_i))^2] \quad (8)$$

$$= \frac{1}{N_c} \sum_{i=1}^{N_c} \mathbb{E}[w_x^2 x_i^2 + w_\beta^2 \beta_\phi(c_i)^2 + 2w_x w_\beta x_i \beta_\phi(c_i)] \quad (9)$$

$$= \frac{1}{N_c} \sum_{i=1}^{N_c} \left[\underbrace{w_x^2 \mathbb{E}[x_i^2]}_{=\mathcal{M}[\mathbf{x}]^2} + \underbrace{w_\beta^2 \mathbb{E}[\beta_\phi(c_i)^2]}_{=\mathcal{M}[\beta_\phi(\mathbf{c})]^2} + 2w_x w_\beta \underbrace{\mathbb{E}[x_i \beta_\phi(c_i)]}_{=0 \text{ (uncorrelated)}} \right] \quad (10)$$

$$= \frac{1}{N_c} \sum_{i=1}^{N_c} [w_x^2 \mathcal{M}[\mathbf{x}]^2 + w_\beta^2 \mathcal{M}[\beta_\phi(\mathbf{c})]^2] \quad (11)$$

$$= w_x^2 \mathcal{M}[\mathbf{x}]^2 + w_\beta^2 \mathcal{M}[\beta_\phi(\mathbf{c})]^2 \quad (12)$$

$$= w_x^2 + w_\beta^2. \quad (13)$$

We then standardize \mathbf{x}_{cond} w.r.t its expected magnitude:

$$\hat{\mathbf{x}}_{\text{cond}} = \frac{\mathbf{c}}{\mathcal{M}[\mathbf{x}_{\text{cond}}]} = \frac{w_x \mathbf{x} + w_\beta \beta_\phi(\mathbf{c})}{\sqrt{w_x^2 + w_\beta^2}}. \quad (14)$$

Karras et al. [19] define w_x and w_β in terms of a blend factor $t \in [0, 1]$ that “can be adjusted on a case-by-case basis”, since (14) is agnostic to the scale of the weights. They choose complementary weights t and $(1-t)$, setting t as a fixed hyperparameter defined empirically. Motivated by FiLM [50], we make this scaling between network activations \mathbf{x} and a conditioning-dependent bias $\beta_\phi(\mathbf{c})$ also learnable and conditioning-dependent. We denote this blend factor as $\gamma_\theta(\mathbf{c})$ due to its conceptual similarity with the scaling in FiLM. γ_θ does not preserve the magnitudes of the input \mathbf{c} . Instead, it leverages a learnable gain and a clamping operation to bound the output in the interval $[0, 1]$.

As our model being pretrained on audio-only data, we want to make the contribution of the condition \mathbf{c} start at zero and progressively increase while retaining the high-quality audio generation capabilities.

Therefore, unlike in FiLM, we initialize the gain in the γ_θ layer at zero and multiply it with β_ϕ instead of x , which here is multiplied with the complement $1 - \gamma_\theta$. We then arrive at the final formulation of MP-FiLM:

$$\text{MP-FiLM}(\mathbf{x}, \mathbf{c} | \theta, \phi) = \frac{(\mathbf{1} - \gamma_\theta(\mathbf{c})) \odot \mathbf{x} + \gamma_\theta(\mathbf{c}) \odot \beta_\phi(\mathbf{c})}{\sqrt{(\mathbf{1} - \gamma_\theta(\mathbf{c}))^2 + \gamma_\theta(\mathbf{c})^2}}. \quad (15)$$

F Computational complexity and sampling speed

On an NVIDIA H100 GPU, generating 1 second of audio takes approximately 8 seconds, while on an Intel Xeon Gold 6240 CPU @ 2.60GHz it takes around 35 seconds (averaged over 10 runs with a warm up run). This includes the whole pipeline, with video and speaker embedding encoders and waveform decoder.

G Details of listening experiment

We conducted two formal listening experiments to assess the performance of *LipDiffuser* and baselines with respect to the aspects of speech quality (i.e. the perceived quality of the generated speech signal) and speaker similarity. The results of each experiment are depicted in Figure 3a and Figure 3b, respectively. Here we provide further information on the experimental setup and other details.

G.1 Experimental setup

The listening experiments were carried out using the browser-based WebMUSHRA⁴ framework. Each experiment consisted of eight trials. In each trial, the participants were presented with a reference audio signal as well as several other audio signals and were asked to rate either the quality or the similarity of each signal compared to the reference. For the reference signals, we randomly sampled clips from *LRS3* and used the pre-enhanced audio tracks (cf. Section 4.1), making sure that each clip comes from a different speaker and that the length of each clip is between 3 seconds and 10 seconds.

Besides the clean reference (labeled as such), the other (unlabeled) audio signals presented largely correspond to Table 1:

- Output of *LipDiffuser*,
- Output of *LipVoicer*,
- Output of *DiffV2S*,
- Output of *IL2S* (with *AV-HuBERT* SSL features),
- Output of *AV-Gen*, based on the noisy audio track from *LRS3-CHiME3* at an SNR of -10 dB,
- The reference itself (as an anchor/sanity check),
- *Only for the speech quality experiment*: the noisy audio track from *LRS3-CHiME3* at an SNR of -10 dB, as a second anchor.

We chose not to include *SGMSE+* and *Lip2Speech* in order to reduce the total listening effort and focus on the better-performing systems according to Table 1. All participants were presented with the same audio clips, but the order of trials as well as the order of signals within each trial were randomized.

Each experiment started with a welcome page containing information and general instructions. This was followed by a training page allowing the participants to familiarize themselves with the browser-based interface and select a comfortable volume level. After finishing the short training, participants proceeded to the trial pages where they were asked to rate the different signals. Participants could play and pause each signal as often as desired and could also limit playback to a certain part of the signal. Rating was done on a continuous scale from 0 to 100 using a slider. Screenshots from the trial pages of both experiments are shown in Figure 6 and Figure 7. All participants took part using high-quality headphones in a quiet room in order to minimize outside influences due to environmental

⁴<https://www.audiolabs-erlangen.de/resources/webMUSHRA>

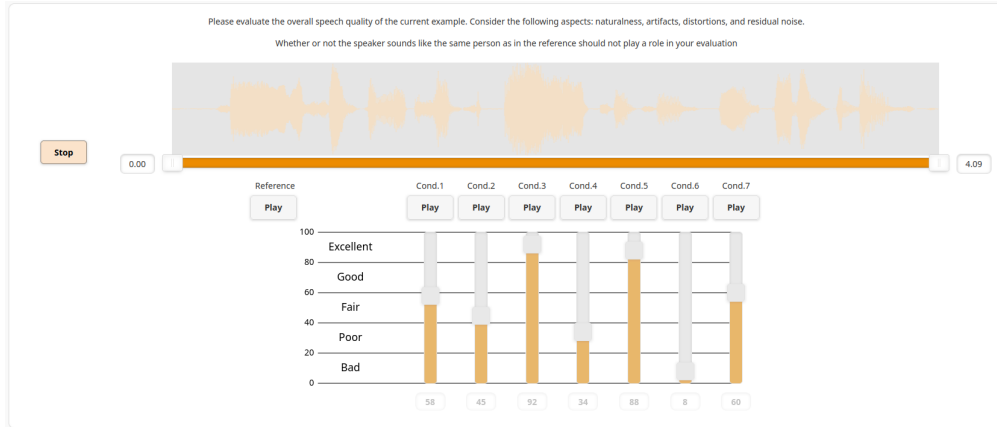


Figure 6: Screenshot of the speech quality listening experiment.

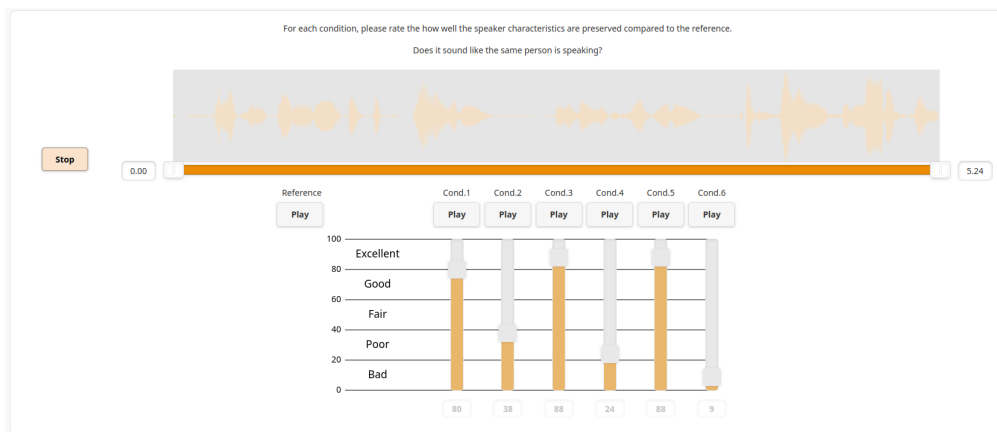


Figure 7: Screenshot of the speaker similarity listening experiment.

noise or other sounds. The experiments were performed in series (speech quality followed by speaker similarity). The overall duration varied between participants but did not exceed one hour.

Participants were instructed to rate the signals using the following texts:

- *Speech quality:*
Please evaluate the overall speech quality of the current example. Consider the following aspects: naturalness, artifacts, distortions, and residual noise. Whether or not the speaker sounds like the same person as in the reference should not play a role in your evaluation.
- *Speaker similarity:*
For each condition, please rate the how well the speaker characteristics are preserved compared to the reference. Does it sound like the same person is speaking?

G.2 Participants and ethical aspects

A group of 15 normal-hearing participants aged 25–37 took part in this experiment. All participants are employed by our institution and took part during working hours. However, participation was not mandated by the institution and each participant could freely decide whether or not to take part without consequences.

All participants have been informed of the purpose of these experiments, the exact procedure and how the collected data will be used. All participants have given their written consent to participating and to the use of their data by signing a detailed consent form prior to taking part.

In the case of studies including human subjects, our institution's ethics board distinguishes between studies which require an ethics vote by the board and studies that do not require such a vote. This is determined by a checklist, which includes items referring to the risks involved, the possibility of anonymizing the collected data, the invasivity of the involved procedures, the vulnerability of participants, and the degree to which participants are able to consent. In our case, all items in the checklist are negative. Hence, according to the regulations of our institution, we are required to conform to all guidelines regarding consent and data protection (which we do), but we do not require an explicit ethics vote or confirmation from the ethics board.